Validation of a strand-level CICC-joint coupling loss model

2012 Supercond. Sci. Technol. 25 025013

(http://iopscience.iop.org/0953-2048/25/2/025013)

Supercond. Sci. Technol. **25** (2012) 025013 (8pp) doi:10.1088/0953-2048/25/2/025013

Validation of a strand-level CICC-joint coupling loss model

E P A van Lanen, J van Nugteren and A Nijhuis

Energy, Materials and Systems, Faculty of Science and Technology, University of Twente, PO Box 217, 7500 AE Enschede, The Netherlands

E-mail: e.p.a.vanlanen@tnw.utwente.nl

Received 8 August 2011, in final form 29 November 2011
Published 22 December 2011
Online at stacks.iop.org/SUST/25/025013

Abstract
Calculating the coupling losses in cable-in-conduit conductor (CICC) joints requires a large amount of numerical effort, which is why the numerical system is often reduced by grouping strands together. However, to better understand the loss behaviour, and eventually the stability mechanism in such joints, a full-sized model working on the level of individual strands is more desirable. For this reason, the numerical cable model JackPot-AC has been expanded to also simulate the coupling losses in a CICC joint. This model has been verified with AC loss measurements on a mock-up joint, which was subjected to an applied harmonic field at different angles. The mock-up joint consisted of two sub-sized CICCs connected by a copper sole. For additional verification the AC loss of one of these conductors and the copper sole was also measured separately. The results of the simulation agree with the measurements, and the model therefore proves to be a useful analytical tool for examining the coupling loss in CICC joints.

(Some figures may appear in colour only in the online journal)

1. Introduction

The twin-box lap-type joint is a type of joint that is recognized for its proven reliability and its suitable assembly, which is why they will be used for the ITER PF coils [1, 2]. However, measurements on sub-sized and full-sized joints for coils have also shown signs of thermal instability when subjected to operating conditions similar to ITER scenarios. These operating conditions involve transient fields within the intended operating range of the coil. It was then that the instabilities were observed as flux jumps in pick-up coil measurements [3, 4]. Due to the transient background field, coupling currents in the strands repeatedly initiated local quenches. Understanding this quench behaviour may contribute in predicting the stability of the whole coil.

Many attempts have been made in the past to estimate the stability of CICC joints by numerical methods in relation to the power dissipation and temperature margin [5–9]. In addition, it is recognized that current imbalance among the strands of a cable can also trigger instability. Since current imbalance is inevitable in a joint, much effort has been spent on predicting this phenomenon with numerical models [10–12]. However, it has proven particularly difficult to simulate full-size ITER-type CICC joints, as they contain many hundreds of superconducting strands. The numerical cable model JackPot-AC was already capable of simulating the interstrand coupling losses in sub-sized CICCs with up to 250 strands and 60 cable intersections [13], and it has recently been upgraded to also simulate the power dissipation in ITER-sized CICCs. The key to this upgrade involves the implementation of the multi-level fast multipole method to cope with the large number of mutual couplings between strand sections [14, 15]. This relieved the considerable computational effort and created the opportunity for a coupling loss model for a full-size ITER CICC joint. Before the full-sized model is established, a sub-sized model has undergone verification by a mock-up joint. This paper describes the details of that verification. The next step is to connect the joint model to a thermohydraulic model to assess the temperature distribution and margin, but this connection will be reported elsewhere.

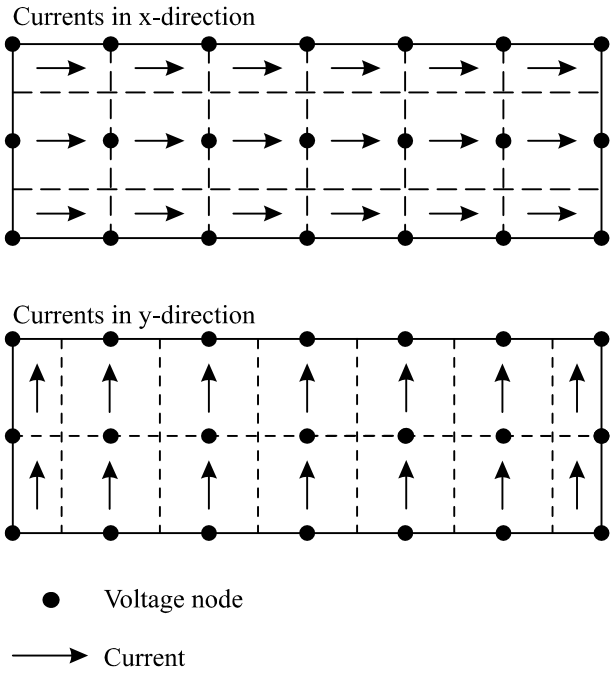

Figure 1. Schematic representation of a 2D rectangular object modelled with the PEEC method.

2. Simulation of the copper sole

The decision on how to model the copper sole of a joint depended heavily on how it could be integrated within the cable model of JackPot-AC. The JackPot-DC model used a finite element (FEM) model, because this has the advantage of allowing different shapes of the sole [16]. However, FEM is not used in JackPot-AC, because it is nearly impossible to include the mutual inductances between strand elements and joint elements. For this purpose, boundary element models or method-of-moments-type models [17] are more suitable. Such models can solve electromagnetic problems on meshes similar to an FEM mesh, but do not require air around the object to be included in the model. The drawback of this method is that it requires extensive implementation efforts, which is why a more straightforward technique is used for the simulation of the joint box. This simulation technique is known as the partial element equivalent circuit (PEEC) method [18]. This method works very well for rectilinear objects and is also easy to implement.

To explain how the PEEC method works, figure 1 shows an object in 2D that is modelled with PEEC. Voltages are calculated on an orthogonal grid across the object, and these nodes are connected with resistors. The value of these resistors is determined by the length and the cross section of the current path between two voltage nodes, as shown in figure 1. The expansion to a 3D model is done in a similar way.

The mutual inductive couplings take place only between those current paths which are parallel to each other. This saves a considerable number of calculations and values to be stored. Between two rectilinear blocks i and j with parallel currents, the mutual inductance is calculated as

$$M_{ij} = \frac{\mu_0 \mathbf{u}_i \cdot \mathbf{u}_j}{4\pi S_i S_j} \int_{V_i} \int_{V_j} \frac{1}{|\mathbf{r}_i - \mathbf{r}_j|} \, \mathrm{d}v_j \, \mathrm{d}v_i, \tag{2.1}$$

where V_i and V_j are the block's volumes, $\mathbf{r}_i$ and $\mathbf{r}_j$ are vectors pointing to locations inside the blocks, $\mathbf{u}_i$ and $\mathbf{u}_j$ are vectors pointing in the direction of the current flow, and S_i and S_j the areas perpendicular to this current flow. Equation (2.1) is rewritten to

$$M_{ij} = \frac{1}{S_i} \int_{V_i} \mathbf{u}_i \cdot \mathbf{A}_{ij} \, \mathrm{d}v_i, \tag{2.2}$$

where

$$\mathbf{A}_{ij}(\mathbf{r}_i, \mathbf{r}_j) = \frac{\mu_0}{4\pi S_j} \int_{V_j} \frac{\mathbf{u}_j}{|\mathbf{r}_i - \mathbf{r}_j|} \, \mathrm{d}v_j. \tag{2.3}$$

If the right-hand side of equation (2.3) is multiplied by the current flowing in object j, its result is the magnetic vector potential at location $\mathbf{r}_i$ due to that current. Equation (2.3) can be solved analytically [19], which reduces the number of volume integrals needed to calculate the mutual inductance from two to one. The solution of this can be found numerically by using, for instance, a Gaussian quadrature or the Simpson rule in three dimensions. Equations (2.2) and (2.3) can also be used to calculate the self-inductance of a block, since the analytical solution of A_{ij} does not contain singularities.

Although the calculation of the mutual inductance is already reduced to one volume integral, the PEEC approach requires it to be solved for a large number of couplings. This still requires a considerable computation time. Some simplifications are allowed if the distance between blocks is large enough. For instance, simplification of equation (2.2) to

$$M_{ij} = \frac{V_i}{S_i} \mathbf{u}_i \cdot \mathbf{A}_{ij}(\mathbf{r}_{i,\mathrm{c}}, \mathbf{r}_j), \tag{2.4}$$

takes away the remaining volume integral. In equation (2.4), $\mathbf{r}_{i,\mathrm{c}}$ is the location of the centre of volume i. For blocks separated even further, equation (2.3) can eventually be approached with

$$\mathbf{A}_{ij}(\mathbf{r}_{i,\mathrm{c}}, \mathbf{r}_{j,\mathrm{c}}) = \frac{\mu_0}{4\pi S_j} \frac{V_j \mathbf{u}_j}{|\mathbf{r}_{i,\mathrm{c}} - \mathbf{r}_{j,\mathrm{c}}|}. \tag{2.5}$$

This does not speed up the computation as much as equation (2.4) but the latter notation has a particular benefit for implementing the multi-level fast multipole method (MLFMM) [14, 15, 20].

To investigate the effect of the simplifications, the mutual inductance is calculated between two equally sized cubes at different distances from each other. Figure 2 shows the configuration and the results. The current density is assumed to be equal everywhere inside the cubes, and the direction of the current flow is perpendicular to the faces indicated with the arrows. The distance is increased in steps equal to the width of the cubes, and the result at distance zero represents the self-inductance of one cube. A four-point 3D Gaussian quadrature formula is used for the solution of the integral in equation (2.2). Of course, for $d/w_x = 0$, which gives the self-inductance of a block, the result for equations (2.4)

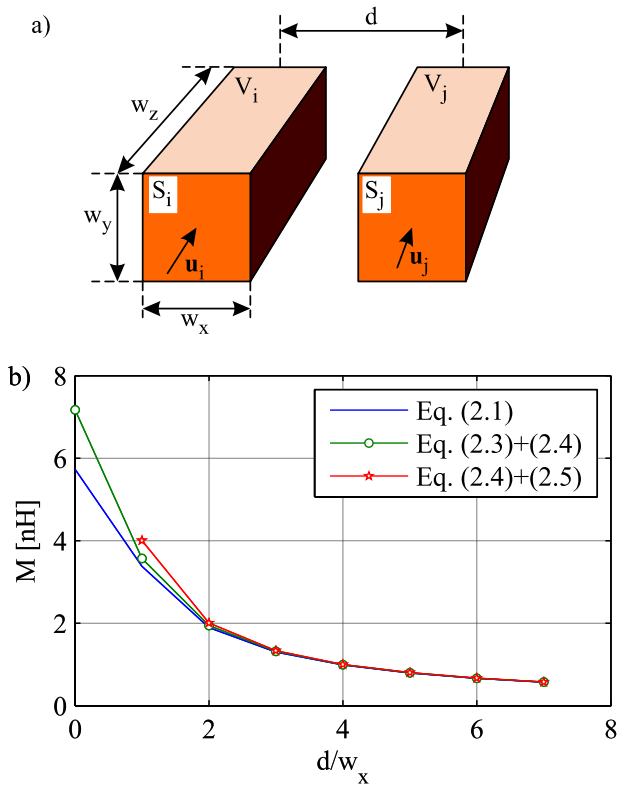

Figure 2. (a) Configuration for the calculation of the mutual inductance and (b) the results for $(w_x, w_y, w_z) = (1, 1, 2)$ cm.

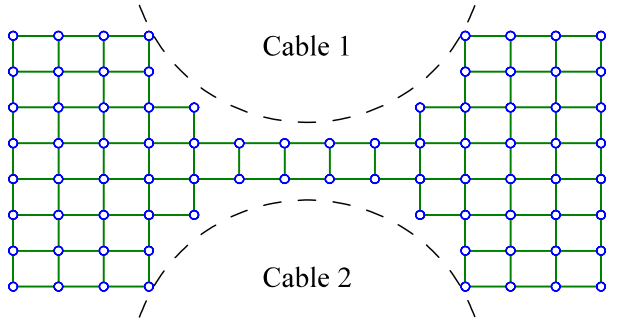

Figure 3. Voltage nodes (circles) and current paths (straight lines) in the cross section of the copper sole as simulated with JackPot-AC.

and (2.5) is undefined because of a division by zero. Based on these results, JackPot-AC uses equation (2.1) for the calculation of the self-inductances and equations (2.4) and (2.5) for the calculation of the mutual inductances between the PEEC blocks.

The notation of the mutual coupling in equation (2.2) has another advantage. If the background field B_{ext} is expressed as magnetic vector potential A_{ext}, the coupling voltage $V_{\text{ext},i}$ for branch i in the circuit simply becomes

$$V_{\text{ext},i} = \frac{1}{S_i}\mathbf{u}_i \cdot \int_{V_i} \partial_t \mathbf{A}_{\text{ext}\,i}\, \mathrm{d}v_i. \tag{2.6}$$

Figure 3 shows the spatial discretization of the copper sole's cross section. It consists of a set of nodes in an orthogonal grid, where the nodes are removed from locations

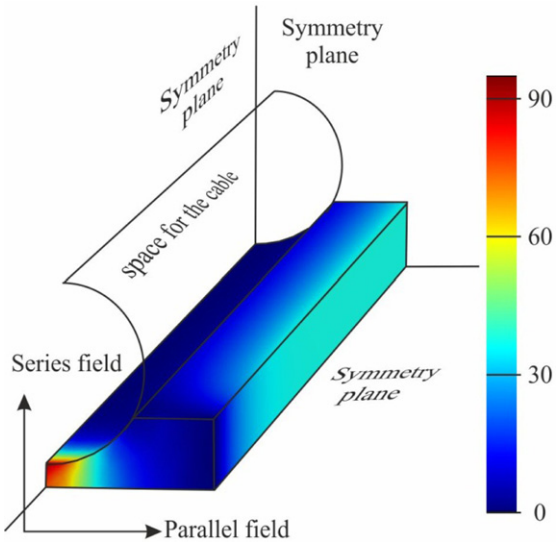

Figure 4. Eddy current loss results from an FEM model of the copper sole. The legend is in mW cm^{-3}.

where the cables would otherwise be located. In addition, the current paths to and from the removed nodes are also taken away from the model to make sure that no sole currents will flow through the cable locations.

The space between nodes in the longitudinal direction of the joint is 1 cm, which is comparable with a typical longitudinal discretization of a cable model in JackPot-AC. This means that the PEEC bars have a relatively large aspect ratio between their longitudinal and cross sectional dimension ratio but this does not affect its behaviour, as is demonstrated in section 3.

3. Determination of the sole's RRR

To determine its RRR, the copper sole has been subjected to eddy current loss measurements at liquid helium temperature in a transverse applied AC magnetic field. This experiment is then simulated with a finite element model in Comsol Multiphysics©, in which the resistivity parameter was adjusted until the simulation results matched the measurements. For completeness, two sets of measurements were done with differently oriented applied AC fields, which are denoted as parallel and series, see figure 4. These denotations refer to the orientation in which the mock-up joint with conductors is placed in the magnetic field. The result in figure 4 was obtained with a harmonic background field in 'series' direction with a frequency of 0.2 Hz and an amplitude of 0.2 T. The RRR in the simulations was adjusted to match the simulated loss with the measurements, which resulted in a RRR of 84. Only 1/8 of the object is simulated to benefit from its threefold symmetry.

Figure 5 shows the results as a function of frequency. Although the maximum frequency used in the measurements was 0.2 Hz, higher frequencies were used in the simulations to compare the behaviour of the JackPot sole with the FEM sole. The results of these models match well with the measurements

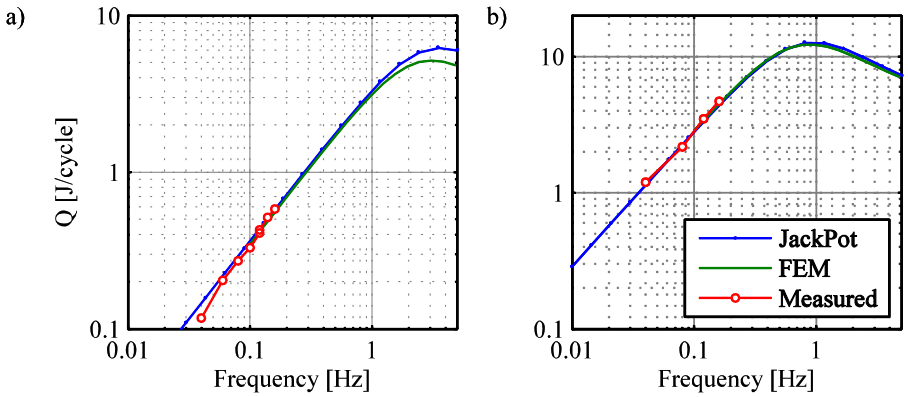

Figure 5. Measurement and simulation results for eddy current losses in the copper sole in a background field with 0.2 T amplitude. The background field is in (a) 'parallel' direction and (b) 'series' direction.

in both orientations of the background field. Even at higher frequencies, the JackPot sole model follows the FEM model's result quite well. This demonstrates the validity of the JackPot sole model.

4. Coupling between the cable and sole models

JackPot-AC can already simulate the coupling losses in a CICC subjected to an applied AC field [13]. Since the current paths of the cables and joints never cross each other by definition (see section 2), the mutual coupling between currents in the joint and the sole are solved with equations (2.4) and (2.5). However, the electrical coupling of the cable model with the copper sole requires special attention, since the modelled sole is obviously not shaped for a cable with a round cross section. For a single cross section, this connection is accomplished in the following three steps, see figure 6.

The first step determines which of the sole's voltage nodes will have a connection with the cable. This is done by considering the dimensions of the PEEC boxes for the z-oriented currents. Note that these dimensions are different for the different orientations of the currents, see figure 1. A box node is only in contact with the cable if the cable overlaps with that box. Once all nodes contacting the cable have been identified, the cable periphery is allocated to a proportional distribution, see figure 6(a). The second step identifies the strands that are in contact with the cable periphery. When combining the results from these two steps, it is possible to identify which strands are in contact with the voltage nodes in the sole. The third and last step involves giving the value of the conductance between strands and the sole in the cross section. This value is determined by their contact area with the cable periphery [21]. A single contact resistivity parameter, ρ_{sj} in $\Omega\ \mathrm{m}^2$, is used for calculating their conductance values.

5. Simulation of a cable in a copper sleeve

For the verification of the model, the mock-up joint was manufactured from two sub-sized CICCs that were connected by a copper sole, which has the scaled dimensions of an

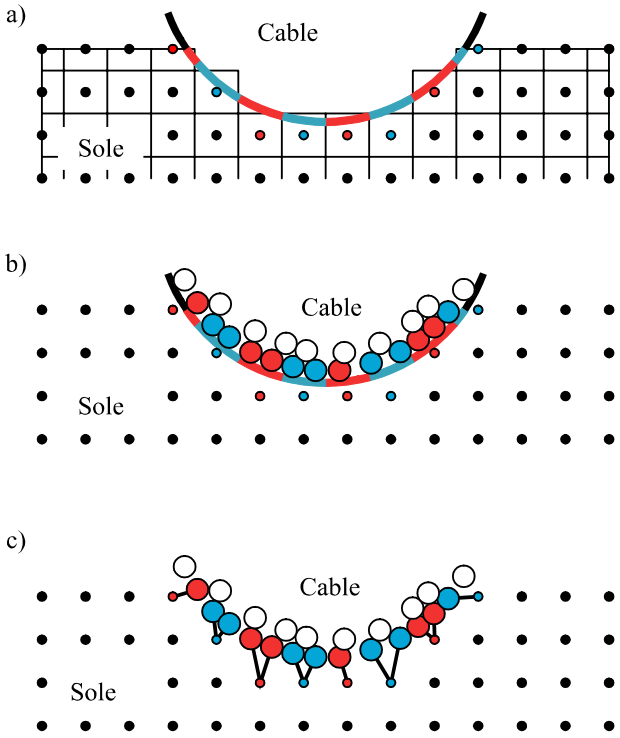

Figure 6. Illustration of the numerical procedure for connecting strands with the sole's voltage nodes.

ITER PF coil joint. The conductors were used before in an experiment to analyse parametric variation of NbTi CICCs where they were denoted as 'NbTi #5' [22, 23]. The conductor sections used for this experiment were compacted in copper sleeves with a 2.5 mm thick wall, which deviates from the ITER PF joint design. One separate sleeved conductor section was also subjected to AC loss measurements for additional verification. Since the influence of the copper sleeve on the measurements cannot be ignored, they were included in the simulations as well. To this end, the sleeves were simulated by placing a single layer of voltage nodes regularly around the conductors, where each node is connected to their neighbours with resistor-inductance paths. Like the sole model described in section 2, the sleeve model has been

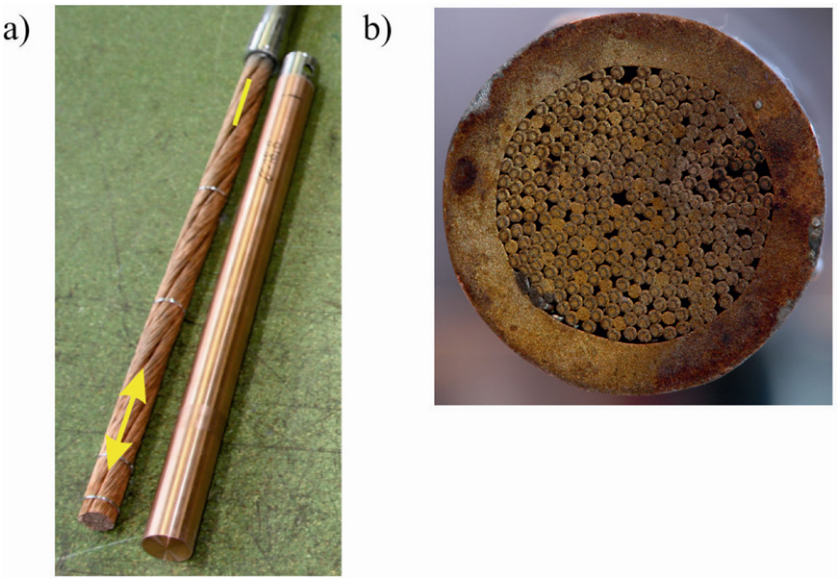

Figure 7. (a) One conductor used for the mock-up joint, before its assembly with a copper sleeve and (b) cross section of this conductor after assembly.

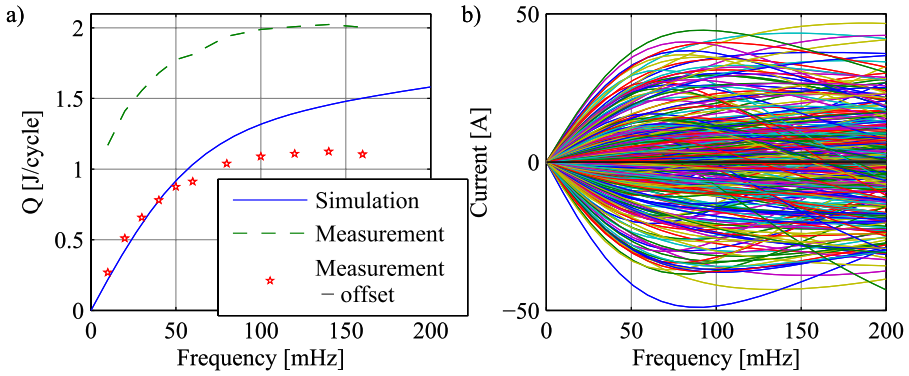

Figure 8. (a) Measured and simulated frequency response of the conductor in figure 7 and (b) simulated strand currents versus frequency in the centre cross section of the cable.

verified with an equivalent FEM simulation. The electrical connection between the cable and the sleeve is performed with the same procedure as described in section 4.

Figure 7 shows the cable and the copper sleeve before and after assembly. Figure 7(a) reveals that the cable untwisted towards the end of the de-sleeved section. For this reason we chose the average value along the cable length for the final-stage twist pitch. Furthermore, the Ni plating had been completely removed from strands at the cable surface, but since the strand bundle was held tightly together with stainless steel wires during removal, the plating is expected to be present between the strand contacts. As such, it is also assumed that the contact resistivity properties are different for strand-to-strand contacts and strand-to-sleeve contacts.

The conductor was measured in a homogeneous AC magnetic field with an amplitude of 0.2 T, ranging in frequency from 0.01 to 0.16 Hz. The usual procedure for obtaining contact resistivity parameters is to fit them with interstrand resistance values from real samples. However, as such data was not available for the particular conductor used in this experiment, the interstrand resistances measured on other conductors were used instead. Previous interstrand resistance and coupling loss simulations were carried out of five sub-sized CICCs consisting of 36 strands, each cable with a different type of strand coating [13]. For the interstrand contact resistance parameter, the value obtained for the sub-sized CICC with Ni plating is used, whereas for the contact resistance between strands and the sleeve, the one without plating (bare copper) is used. In addition, the final-stage twist pitch in the simulation was determined as twice the nominal value given for this conductor due to the untwisting.

Figure 8 shows the results of both the measurements and the simulation. For the sake of convenience, figure 8(a) also shows the measured result where an offset of 0.9 J/cycle has been subtracted from the measurements. This is the constant factor in a polynomial fit of the measured data, which represents the hysteresis loss in the strands at low frequency. Although the AC loss for a CICC is usually given per unit superconductor volume, this is not done here. The reason is

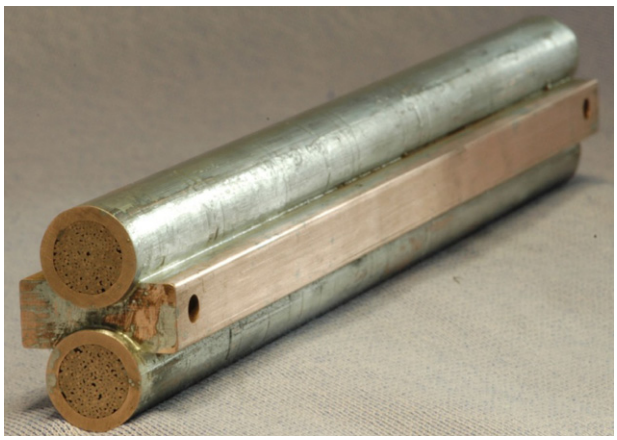

Figure 9. The mock-up joint assembly.

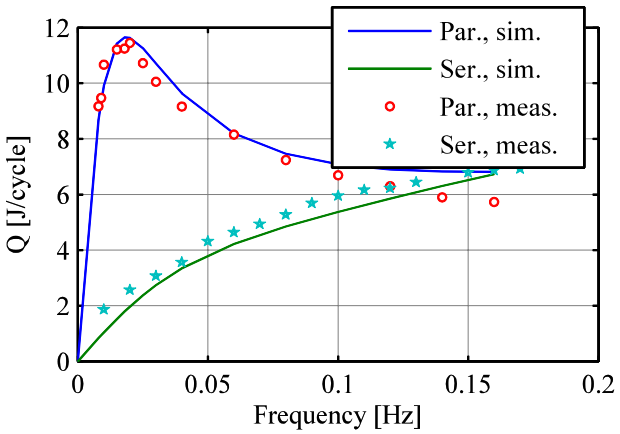

Figure 10. Measured and simulated AC loss of the joint versus frequency, under different angles of the applied AC field.

that, in this way, it is easier to distinguish the loss components of the sole, cables and the whole joint. Had the displayed loss been divided by the superconducting strand volume, the offset would have been 95 mJ/(cycle cm^3).

The measured loss shows saturation at about 140 mHz, whereas the saturation in the simulation appears to be at a much higher frequency and amplitude. It is unlikely that this is the result of strands being driven into saturation—this effect is not taken into account in the simulations—because the strand currents are too low for that, see figure 8(b). For now, the reason behind the difference between the measured and simulated loss at higher frequencies remains unknown.

6. Simulation of the mock-up joint

Figure 9 depicts the assembly of the mock-up joint. Similar to the cable measurements described in section 5, the measurement on the joint was also carried out in a homogeneous applied AC field with an amplitude of 0.2 T and a frequency ranging from 0.01 to 0.16 Hz. Figure 10 shows the results for both the parallel and series background field orientations. This time, no offset has been subtracted from the measured data to account for hysteresis loss. The reason is that, already at low frequencies, the field is starting to be screened from the inside of the conductor, see figure 11. This alters the overall hysteresis loss in the conductors, which makes it incorrect to assume it is constant over the frequency range used.

A remarkable observation is that the simulated joint loss matches the measured results better than the simulated conductor loss of section 5. The explanation is that the interstrand coupling loss in the joint is only a small component of the overall loss. On the other hand, the eddy current loss can be simulated much better than the coupling losses, and they are more dominant in the results. This is illustrated in figure 12, which shows the contributions from the power dissipation due to the cable interstrand coupling loss; the coupling contacts between the cable and the copper sleeve and the Joule heating in the sole separately.

Figure 12 also shows that the loss in the interstrand contact resistances and the strand-to-sleeve resistances is almost equal. However, contrary to the other loss components, the power in the contact between the cables and sleeves is dissipated in a small layer, leading to a particularly high power density. Analysis of what the effect of this would be on the local temperature distribution inside the cable requires

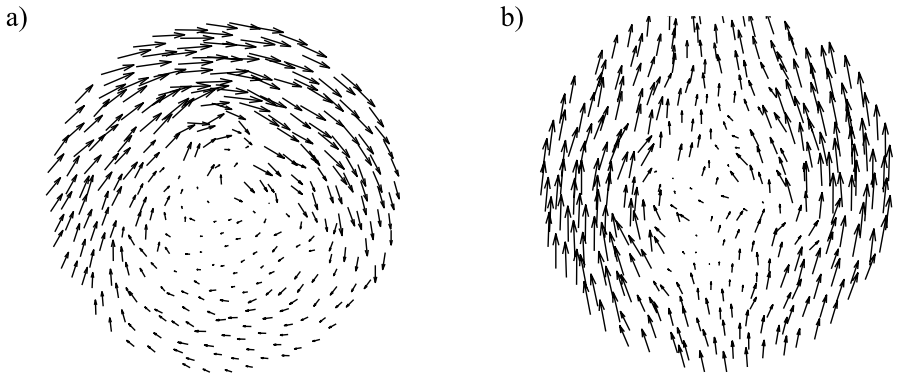

Figure 11. Simulated magnetic field at the location of strands in the central cross section of the upper conductor at a frequency of 50 mHz in (a) parallel background field and (b) series background field.

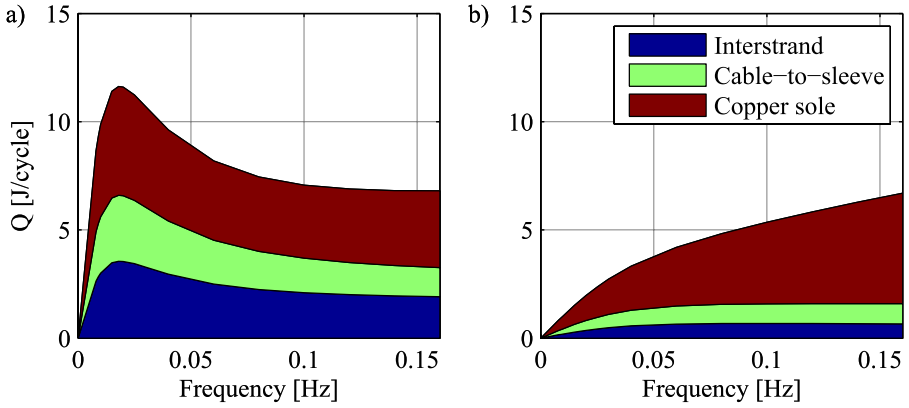

Figure 12. Different sources of the simulated coupling loss versus frequency in (a) parallel background field and (b) series background field.

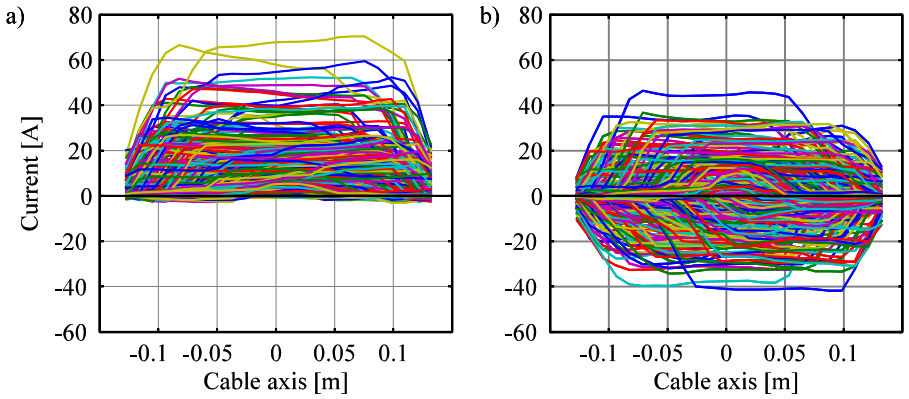

Figure 13. Strand currents in the centre of one of the cables at (a) 20 mHz in the parallel background field and (b) 60 mHz in the series background field.

the implementation of a thermohydraulic model and is still ongoing.

Another feature which the model allows us to analyse is the distribution of strand currents. Figure 13 illustrates this for the two different AC field orientations, each at one frequency. The result for the 'parallel' applied AC field is biased to a positive current due to the coupling currents flowing between the cables. The currents in the opposite conductor attached to the joint (not shown here) are biased to a negative current. Another observation is that both orientations show that strand currents change rapidly along short lengths and change slowly over much longer lengths. This indicates that the current transfer mostly takes place between strands that are in contact with the copper sleeve, due to the lower strand-to-sleeve contact resistances compared to the interstrand resistances.

7. Conclusions

The numerical model for calculating interstrand coupling losses in cable-in-conduit conductors (CICCs), JackPot-AC, has been expanded with an effective copper sole model. Similar to the cable model, the copper sole model is a network of resistors, self-inductances, mutual inductances and voltage sources controlled by an externally applied field, which facilitates its integration with JackPot-AC. To verify the model, a mock-up joint (scaled to the present ITER PF joint design) has been manufactured on which AC loss measurements have been carried out with two orientations of the applied AC field. The model uses, besides the geometry of the joint components and the cable twist pitches, three input parameters for the computation, which are: the cable interstrand contact resistance; the contact resistance between strands and the copper sole resistivity.

The model is able to reproduce the measurement results with good accuracy and allows to extract information about the electrical behaviour of the joint that is not revealed by the measurements. The simulation of this particular case demonstrates that a considerable amount of energy is dissipated in the copper parts of the joint due to eddy currents. In addition, a high energy density is found in the contacts between the cable and the copper sole, which may lead to a local rise of temperature. After implementation of the thermohydraulic part, the model provides a solid basis for detailed optimization of CICC joints.

Acknowledgments

This work was supported by ITER IO, Cadarache, France within the framework of the ITER Service contract no. UT-ITER/CT/09/4300000070. The authors are grateful to

P L Bruzzone from CRPP, Villigen, Switzerland, for providing the conductors that were required to manufacture the mock-up joint.

References

[1] Mitchell N, Bessette D, Gallix R, Jong C, Knaster J, Libeyre P, Sborchia C and Simon F 2008 The ITER magnet system *IEEE Trans. Appl. Supercond.* **18** 435–40

[2] Lim B, Simon F, Ilyin Y, Gung C Y, Smith J, Hsu Y H, Luongo C, Jong C and Mitchell N 2011 Design of the ITER PF coils *IEEE Trans. Appl. Supercond.* **21** 1918–21

[3] Zani L, Decool P, Cloez H, Serries J P and Bej Z 2003 Manufacture and test of NbTi subsize joint samples for the ITER poloidal field coils *IEEE Trans. Appl. Supercond.* **13** 1460–3

[4] Zanino R *et al* 2009 EU contribution to the test and analysis of the ITER poloidal field conductor insert and the central solenoid model coil *Supercond. Sci. Technol.* **22** 085006

[5] Ciazynski D and Martinez A 2002 Electrical and thermal designs and analyses of joints for the ITER PF coils *IEEE Trans. Appl. Supercond.* **12** 538–42

[6] Bellina F and Ghin M 1999 Methods for the analysis of the joints between superconducting cables *IEEE Trans. Appl. Supercond.* **9** 189–92

[7] Fresa R, Rubinacci G, Ventre S, Villone F and Zamboni W 2009 Fast solution of a 3D integral model for the analysis of ITER superconducting coils *IEEE Trans. Magn.* **45** 988–91

[8] Albanese R, Fresa R, Portone A, Rubinacci G, Villone F and Zamboni W 2006 Analysis of resistive joints for superconducting cables for fusion applications *IEEE Trans. Magn.* **42** 1355–8

[9] Portone A, Rubinacci G, Villone F and Zamboni W 2007 Electromagnetic 3D analysis of an ITER full-size cable-in-conduit conductor sample *Supercond. Sci. Technol.* **20** 1032–45

[10] Breschi M, Fabbri M, Negrini F and Ribani P L 2003 Combined modeling of cables and joints/terminations for the electromagnetic analysis of superconducting cables *IEEE Trans. Appl. Supercond.* **13** 2400–3

[11] Seo K, Mito T, Miller J R, Kawabata S, Ichihara T and Hasegawa M 2005 Analysis of joint-resistance-induced, non-uniform current distribution *IEEE Trans. Appl. Supercond.* **15** 1595–8

[12] Zanino R, Bagnasco M, Bellina F, Gislon P, Ribani P L and Savoldi Richard L 2005 Modeling AC losses in the ITER NbTi poloidal field full size joint sample (PF-FSJS) using the THELMA code *Fusion Eng. Des.* **75–79** 23–7

[13] Van Lanen E P A and Nijhuis A 2011 Simulation of interstrand coupling loss in cable-in-conduit conductors with JackPot-AC *IEEE Trans. Appl. Supercond.* **21** 1926–9

[14] Greengard L F 1988 *The Rapid Evaluation of Potential Fields in Particle Systems* (Cambridge, MA: MIT Press)

[15] Gumerov N A and Duraiswami R 2005 *Fast Multipole Methods for the Helmholz Equation in Three Dimensions* (Oxford: Elsevier)

[16] Van Lanen E P A and Nijhuis A 2011 Numerical analysis of the DC performance of ITER TF samples with different cabling pattern based on resistance measurements on terminations *Supercond. Sci. Technol.* **24** 085010

[17] Gibson W C 2008 *The Method of Moments in Electromagnetics* (Boca Raton, FL: Chapman and Hall/CRC Press)

[18] Ekman J 2003 Electromagnetic modeling using the partial element equivalent circuit method *Dept. of Computer Science and Electrical Engineering* (Lulea: Lulea University of Technology) Available at http://staff.www.ltu.se/~jekman/Pres/PhDThesis.pdf

[19] Bellina F and Serra E 2004 Computation of the magnetostatic field by means of a mixed analytical-numerical procedure *IEEE Trans. Magn.* **40** 834–7

[20] Yokota R and Barba A 2011 Treecode and fast multipole method for N-body simulation with CUDA, arXiv:1010.1482v1

[21] van Lanen E P A and Nijhuis A 2009 JackPot: a novel model to study the influence of current non-uniformity and cabling patterns in cable-in-conduit conductors *Cryogenics* **50** 139–48

[22] Wesche R, Anghel A, Stepanov B and Bruzzone P 2004 DC performance of subsize NbTi cable-in-conduit conductors *IEEE Trans. Appl. Supercond.* **14** 1499–502

[23] Wesche R, Anghel A, Stepanov B, Vogel M and Bruzzone P 2005 DC performance, AC loss and transient field stability of five medium size NbTi cable-in-conduit conductors with parametric variation *Cryogenics* **45** 755–79